

## Electronic Supplementary Information

### Amorphous-mediated crystallization of calcium pyrophosphate tetrahydrate: the role of alkaline earth metal ions

Shiwen Cui,<sup>a</sup> Yuan Su<sup>a,b\*</sup> and Ting Cai<sup>a,c\*</sup>

<sup>a</sup> Department of Pharmaceutics, School of Pharmacy, China Pharmaceutical University, Nanjing 210009, China

<sup>b</sup> Department of Pharmaceutical Engineering, School of Engineering, China Pharmaceutical University, Nanjing 210009, China

<sup>c</sup> State Key Laboratory of Natural Medicines, China Pharmaceutical University, Nanjing 210009, China

**Figure S1.** TGA curves of the precipitates at S1(black line) and S3(red line).

**Figure S2.** Representative calcium and pH curves in the presence of metal-ion additives at different concentrations: (a) Mg<sup>2+</sup>; (b) Sr<sup>2+</sup>; and (c) Ba<sup>2+</sup>. The black curves represent the control experiments in all groups.

**Figure S3.** (a) XRD patterns, (b) Raman spectra and (c) TGA curves of the crystalline precipitates at the stage 3 in the presence of 0.2 mM Mg<sup>2+</sup>, 0.2 mM Sr<sup>2+</sup>, 0.2 mM Ba<sup>2+</sup>, indicating no other phases except the CPPT.

**Figure S4.** Time-development calcium consumption during CPPT growth in the presence of (a) Ba<sup>2+</sup> (b) Sr<sup>2+</sup> and (c) Mg<sup>2+</sup> at various concentrations.

**Figure S5.** The change in induction time of ACPPT crystallization in the presence of (a) Sr<sup>2+</sup> and (b) Ba<sup>2+</sup> introduced by premixing or postmixing.

**Figure S6.** TEM images of the precipitates at the late stage of the first period (45min), the thin sheet-like phases surrounding the amorphous agglomerates were marked by the yellow squares. The sheet-like phases were elongated, and their straight edges were marked by white dashed lines.

**Table S1.** The reaction and the equilibrium constants of complexes input into the calculation.

**Table S2.** The concentrations of pyrophosphate species in the presence and absence of 0.2 mM Mg<sup>2+</sup>.

**Table S3.** The data of hydration energy and water exchange constant of metal ions from the literature.

#### Supplementary Methods:

Calculation of solute species composition

Correlation Analysis

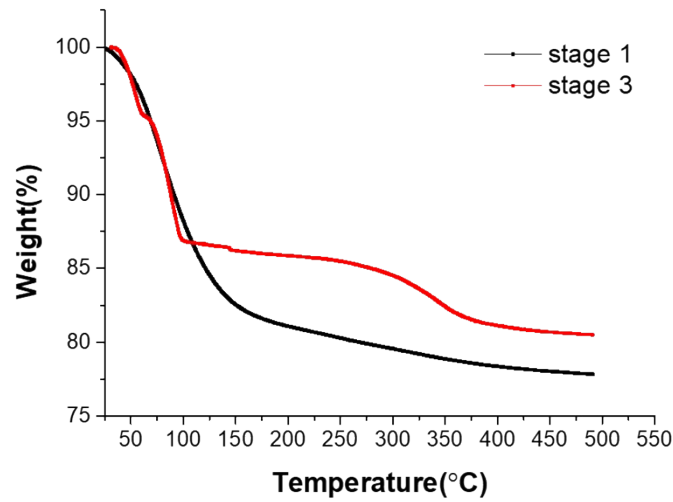


**Figure S1.** TGA curves of the precipitates at S1(black line) and S3(red line).

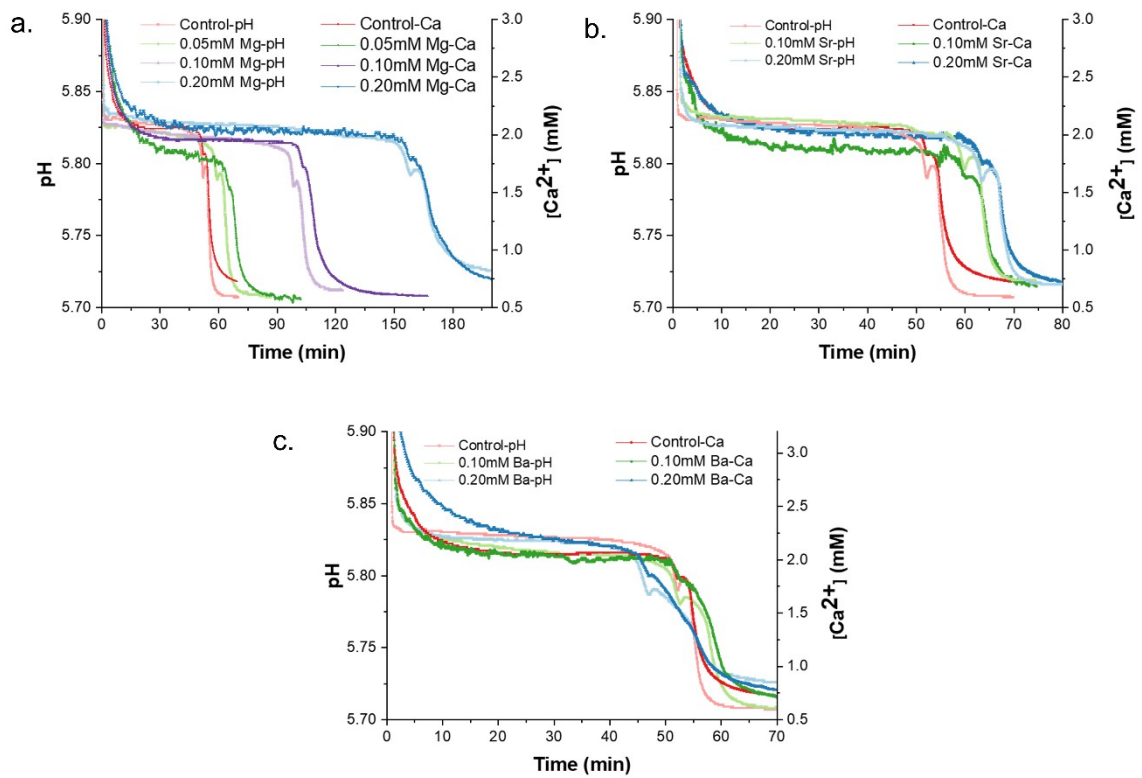


**Figure S2.** Representative calcium and pH curves in the presence of metal-ion additives at different concentrations: (a)  $Mg^{2+}$ ; (b)  $Sr^{2+}$ ; and (c)  $Ba^{2+}$ . The black curves represent the control experiments in all groups.

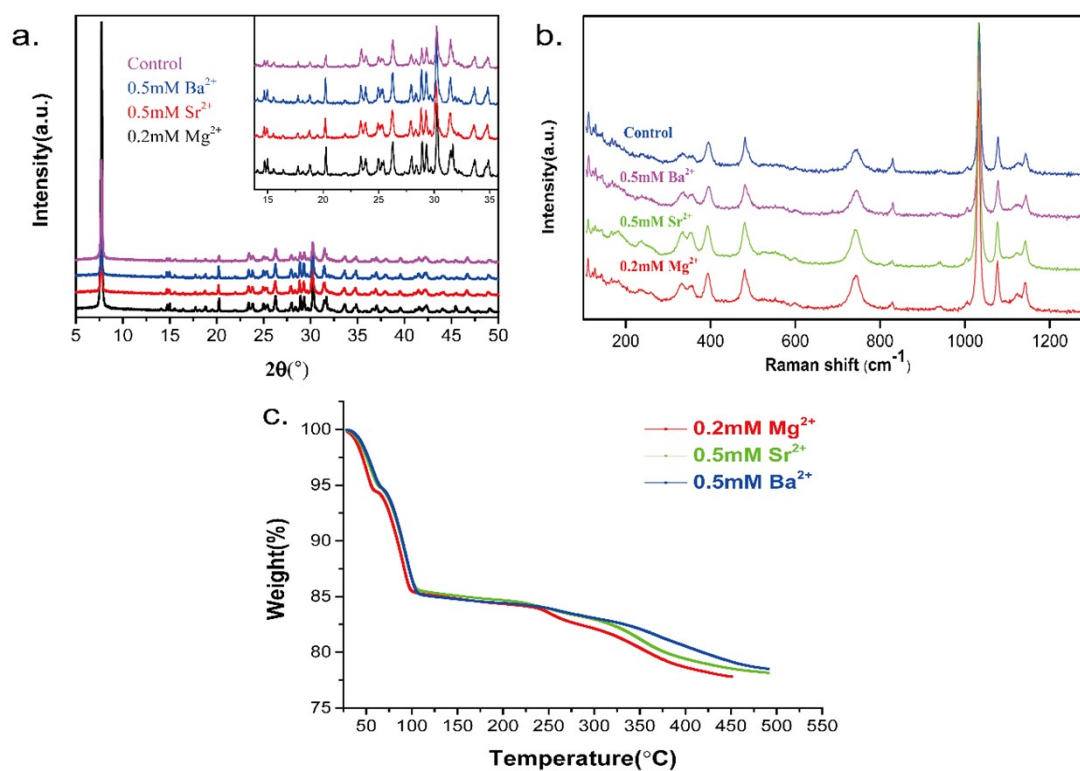


**Figure S3.** (a) XRD patterns, (b) Raman spectra and (c) TGA curves of the crystalline precipitates at the stage 3 in the presence of 0.2 mM  $\text{Mg}^{2+}$ , 0.2 mM  $\text{Sr}^{2+}$ , 0.2 mM  $\text{Ba}^{2+}$ , indicating no other phases except the CPPT.

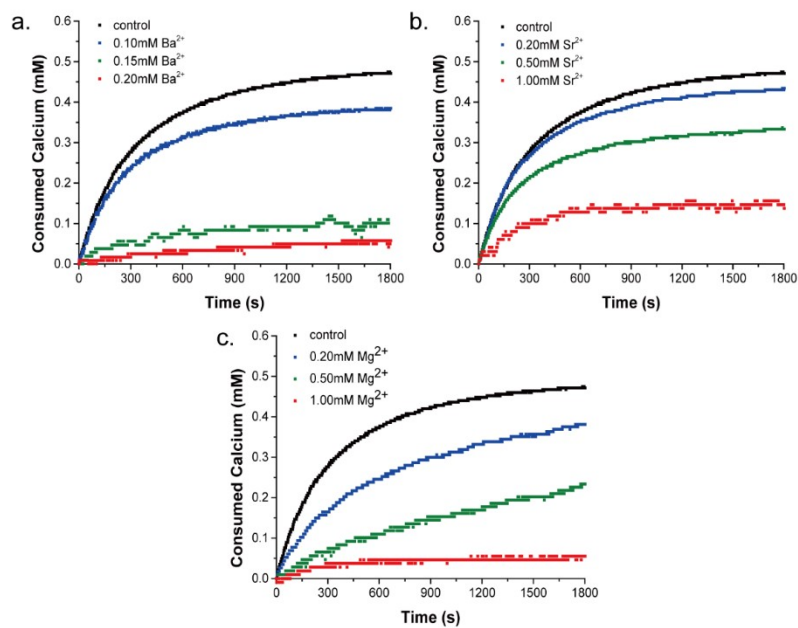


**Figure S4.** Time-development calcium consumption during CPPT growth in the presence of (a)  $\text{Ba}^{2+}$  (b)  $\text{Sr}^{2+}$  and (c)  $\text{Mg}^{2+}$  at various concentrations.

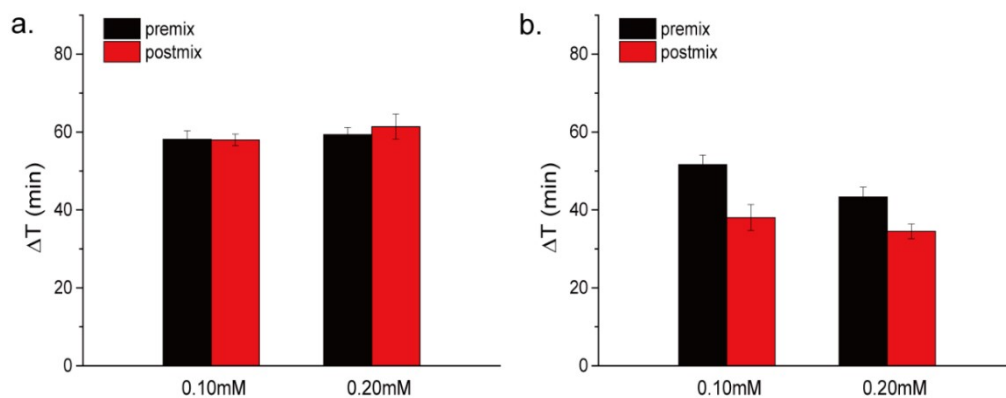


**Figure S5.** The change in induction time of ACPP crystallization in the presence of (a)  $\text{Sr}^{2+}$  and (b)  $\text{Ba}^{2+}$  introduced by premixing or postmixing.

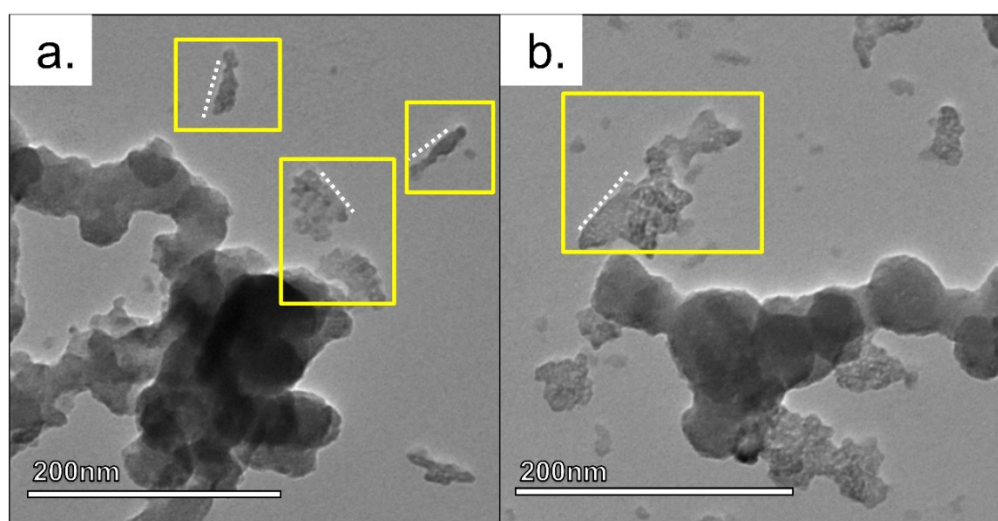


**Figure S6.** TEM images of the precipitates at the late stage of the first period (45min), the thin sheet-like phases surrounding the amorphous agglomerates were marked by the yellow squares. The sheet-like phases were elongated, and their straight edges were marked by white dashed lines.

	Reaction	logK
$\{H_xP_2O_7^y\}_{total}$	$H^+ + P_2O_7^{-4} = HP_2O_7^{-3}$	9.6 <sup>1</sup>
	$H^+ + HP_2O_7^{-3} = H_2P_2O_7^{-2}$	6.7 <sup>1</sup>
	$H^+ + H_2P_2O_7^{-2} = H_3P_2O_7^{-}$	2.0 <sup>1</sup>
	$H^+ + H_3P_2O_7^{-} = H_4P_2O_7$	1.5 <sup>1</sup>
$\{Ca_xH_yP_2O_7^z\}_{total}$	$Ca^{2+} + P_2O_7^{-4} = CaP_2O_7^{-2}$	6.5 <sup>1</sup>
	$Ca^{2+} + HP_2O_7^{-3} = CaHP_2O_7^{-}$	4.3 <sup>1</sup>
	$Ca^{2+} + H_2P_2O_7^{-2} = CaH_2P_2O_7$	2.7 <sup>1</sup>
$\{Mg_xH_yP_2O_7^z\}_{total}$	$Mg^{2+} + P_2O_7^{-4} = MgP_2O_7^{-2}$	7.1 <sup>2</sup>
	$2Mg^{2+} + P_2O_7^{-4} = Mg_2P_2O_7$	2.4 <sup>3</sup>
	$Mg^{2+} + HP_2O_7^{-3} = MgHP_2O_7^{-}$	12.8 <sup>4</sup>

e equilibrium constants were taken from the corresponding literature. <sup>1-4</sup>

**Table S1.** The reaction and the equilibrium constants of complexes input into the calculation.

### Supplementary Table S2

	$\{H_xP_2O_7^y\}_{total}$ (mM)	$\{Ca_xH_yP_2O_7^z\}_{total}$	$\{Mg_xH_yP_2O_7^z\}_{total}$	Sat.Index (CPPT) <sup>a</sup>
Control	1.23	1.27	-	3.20
0.2mM Mg <sup>2+</sup>	1.11	1.39	0.20	3.17

a. Log<sub>K<sub>sp</sub></sub>(CPPT)=17.1, is obtained from ref 1.

**Table S2.** The concentrations of pyrophosphate species in the presence and absence of 0.2 mM Mg<sup>2+</sup>.

### Supplementary Table S3

		the molar Gibbs energies of hydration of ions <sup>5</sup> (kJ/mol)	the logarithm value of water exchange rate constant (1/s)
Alkaline Earthe Metals	Mg <sup>2+</sup>	-1830	5.42 <sup>6</sup>
	Sr <sup>2+</sup>	-1380	8.60 <sup>7</sup>
	Ba <sup>2+</sup>	-1250	9.10 <sup>6</sup>
	Mn <sup>2+</sup>	-1760	7.36 <sup>8, 9</sup>
Transition Metals	Cu <sup>2+</sup>	-2010	9.08 <sup>6</sup>
	Co <sup>2+</sup>	-1915	6.33 <sup>9, 10</sup>
	Fe <sup>3+</sup>	-4265	3.08 <sup>10</sup>
	Ni <sup>2+</sup>	-1980	4.50 <sup>10</sup>
Group IIIA Metals	V <sup>3+</sup>	-4220	3.20 <sup>10</sup>
	Al <sup>3+</sup>	-4525	-0.80 <sup>10</sup>
	In <sup>3+</sup>	-3980	4.30 <sup>10</sup>
Lanthanides	La <sup>3+</sup>	-3145	8.30 <sup>11, 12</sup>
	Ce <sup>3+</sup>	-3200	8.50 <sup>11</sup>
	Gd <sup>3+</sup>	-3375	8.94 <sup>11</sup>

**Table S3.** The data of hydration energy and water exchange constant of metal ions from the literature.

## Supplementary Methods

### Calculation of solute species composition

The composition and activities of solute species were calculated by PHREEQC Interactive 3.1 with the Minteq v4 database. The Davies modified equation was used to calculate the activity coefficients with a b parameter of 0.3. The equilibrium constants of complexes absence in the database were shown in Table S1. The calculation of solute species composition in the presence of 0.2mM Mg<sup>2+</sup> and the control group was shown in Table S2. The decrease of the available pyrophosphate species concentration was not significant after adding magnesium.

### Correlation Analysis

To test the proposed model, we selected more types of metal ions and determined the induction time of ACPP in the presence of those metal ions. The hydration properties of metal cations can be quantitatively described by several thermodynamic and kinetics parameters. Here, the free energy of ionic hydration and water exchange rate constant were taken into consideration according to the literatures. The water exchange rate constant was defined as the reciprocal of the mean residence time of the water molecule in the first hydration shell determined by various experimental methods combined with computer

simulations, which might cause the deviation.<sup>13</sup> Nevertheless, the water residence time in the first hydration shell of each metal ion ranged across almost 20 orders of magnitude from picosecond to years, which makes the comparison between the ions plausible.<sup>14</sup>

As shown in Fig.5a, the hydration free energy of cations was positively correlated with the corresponding induction time and in line with our assumption except for the lanthanides. The Pearson correlation coefficient was only 0.70 while the value was 0.92 by removing the  $\text{La}^{3+}$ ,  $\text{Ce}^{3+}$ , and  $\text{Gd}^{3+}$ . However, the deviation was not observed in the correlation with the water exchange rate constant. We suspected that the inconsistency in the thermodynamic and kinetic properties of lanthanide ionic hydration caused the deviation. In fact, there are 9- and 8-coordinated lanthanide hydrated species coexisting with relatively high exchange frequency. The low energy barrier between 8- and 9-fold coordinated species cause the lability of the first hydration shell structure and hence high water exchange dynamics.<sup>15</sup> The water residence times of lanthanides are rather short compared to other trivalent metal ions, despite their high charge density which attracts the water molecules (e.g.,  $\sim 5\text{ns}$  for  $\text{La}^{3+}$ ,  $\sim 6\text{s}$  for  $\text{Al}^{3+}$ ).<sup>12, 16</sup> These results indicated that both thermodynamic and kinetic factors of hydration played roles in inhibiting surface crystallization. The hydrated cations with thermodynamic and kinetic stability would provide better shielding effect, such as  $\text{Al}^{3+}$  and  $\text{Fe}^{3+}$ .

It is noteworthy that there is a certain degree of association between hydration energies and water dynamics in the hydration shell for most of the metal ions. The reason is that they are both based on the electrostatic interaction between metal ions and water molecules, however, the interrelation is much more complex. The order is not always followed that the water molecules in the hydration shell of cations with higher hydration energy will bind tightly and exchange slowly. Besides the lanthanides, other cations with hydration energy similar or even slightly higher to  $\text{Mg}^{2+}$ , such as  $\text{Mn}^{2+}$  and  $\text{Cu}^{2+}$ , did not prolong the induction time more obviously either. It could also interpret by the difference between the hydration shell exchange dynamics. As shown in Fig. 9b, the water exchange constant of  $\text{Mg}^{2+}$  is the lowest among them. The finding suggested that the dynamics characteristics of metal-ion hydration were involved in regulating the crystallization process. It may provide an additional explanation on why  $\text{Mg}^{2+}$  is so unique in modulating the crystallization kinetics of amorphous precursors, such as calcium carbonate and calcium phosphate.

## Supplementary Reference

- 1 M. R. Christoffersen, T. Balic-Zunic, S. r. Pehrson and J. r. Christoffersen, *J. Cryst. Growth*, 2000, **212**, 500-506.
- 2 J. Inczedy, *Równowagi kompleksowania w chemii analitycznej*, Państwowe Wydaw. Naukowe, 1979.
- 3 J.-H. Klemme and H. Gest, *Proc. Nat. Acad. Sci.*, 1971, **68**, 721-725.
- 4 V. W.-H. Leung and B. W. Darvell, *J. Dent.*, 1997, **25**, 475-484.

- 5 Y. Marcus, *J. Chem. Soc., Faraday Trans.*, 1991, **87**, 2995-2999.
- 6 J. Burgess, *Ions in solution: basic principles of chemical interactions*, Woodhead Publ, Oxford, 2nd ed., Repr edn., 2011.
- 7 Y. Marcus, *Ions in Solution and their Solvation*, John Wiley & Sons, 2015.
- 8 R. Aakesson, L. G. Pettersson, M. Sandstroem and U. Wahlgren, *J. Am. Chem. Soc.*, 1994, **116**, 8705-8713.
- 9 H. Eyring, D. Henderson and W. Jost, *Physical Chemistry: An Advanced Treatise*, Academic Press New York, London, 1967.
- 10 J. Burgess, in *Ions in Solution*, ed. J. Burgess, Woodhead Publishing, 1999, pp. 111-123.
- 11 D. P. Fay, D. Litchinsky and N. Purdie, *The Journal of Physical Chemistry*, 1969, **73**, 544-552.
- 12 N. Purdie and C. A. Vincent, *Trans. Faraday Soc.*, 1967, **63**, 2745.
- 13 L. Helm and A. E. Merbach, *Coord. Chem. Rev.*, 1999, **187**, 151-181.
- 14 L. Helm and A. E. Merbach, *CHIMIA International Journal for Chemistry*, 2019, **73**, 179-184.
- 15 M. Duvail, R. Spezia and P. Vitorge, *ChemPhysChem*, 2008, **9**, 693-696.
- 16 C. Beuchat, D. Hagberg, R. Spezia and L. Gagliardi, *J. Phys. Chem. B*, 2010, **114**, 15590-15597.